JBC RESEARCH ARTICLE

Complex interplay between FMRP and DHX9 during DNA replication stress

Received for publication, June 7, 2023, and in revised form, November 28, 2023 Published, Papers in Press, December 16, 2023,
https://doi.org/10.1016/j.jbc.2023.105572

Arijita Chakraborty[1,‡], Arijit Dutta[2,‡], Leonardo G. Dettori[1], Rosemarie Daoud[1], Jing Li[1], Leticia Gonzalez[3], Xiaoyu Xue[3], Heidi Hehnly[4], Patrick Sung[2], Alaji Bah[1], and Wenyi Feng[1,*]

From the [1]Department of Biochemistry and Molecular Biology, SUNY Upstate Medical University, Syracuse, New York, USA; [2]Department of Biochemistry and Structural Biology, University of Texas Health Science Center San Antonio, San Antonio, Texas, USA; [3]Department of Chemistry and Biochemistry, Texas State University, San Marcos, Texas, USA; [4]Department of Biology, Syracuse University, Syracuse, New York, USA

Reviewed by members of the JBC Editorial Board. Edited by Craig Cameron

Mutations in, or deficiency of, fragile X messenger ribonucleoprotein (FMRP) is responsible for the Fragile X syndrome (FXS), the most common cause for inherited intellectual disability. FMRP is a nucleocytoplasmic protein, primarily characterized as a translation repressor with poorly understood nuclear function(s). We recently reported that FXS patient cells lacking FMRP sustain higher level of DNA double-strand breaks (DSBs) than normal cells, specifically at sequences prone to forming R-loops, a phenotype further exacerbated by DNA replication stress. Moreover, expression of FMRP, and not an FMRPI304N mutant known to cause FXS, reduced R-loop-associated DSBs. We subsequently reported that recombinant FMRP directly binds R-loops, primarily through the carboxyl terminal intrinsically disordered region. Here, we show that FMRP directly interacts with an RNA helicase, DHX9. This interaction, which is mediated by the amino terminal structured domain of FMRP, is reduced with FMRPI304N. We also show that FMRP inhibits DHX9 helicase activity on RNA:DNA hybrids and the inhibition is also dependent on the amino terminus. Furthermore, the FMRPI304N mutation causes both FMRP and DHX9 to persist on the chromatin in replication stress. These results suggest an antagonistic relationship between FMRP and DHX9 at the chromatin, where their proper interaction leads to dissociation of both proteins from the fully resolved R-loop. We propose that the absence or the loss of function of FMRP leads to persistent presence of DHX9 or both proteins, respectively, on the unresolved R-loop, ultimately leading to DSBs. Our study sheds new light on our understanding of the genome functions of FMRP.

Fragile X syndrome (FXS) is a neurodevelopmental disorder due to epigenetic silencing or loss-of-function mutations of the *FMR1* gene encoding fragile X messenger ribonucleoprotein (FMRP) (1, 2). FMRP is a nuclear-cytoplasmic RNA binding protein that regulates multiple biological processes of its diverse mRNA substrates, including their maturation in the nucleus, nuclear export, cytoplasmic transport, and ultimately, their translation at the synapse (3–5). The ability of FMRP to participate in multiple processess in the cell is attributed to the presence of multiple domains and their relative 3D-organization. All FMRP splice variants contain two amino (N-) terminal methylated lysine-binding Agenet domains (Age1 and Age2), three K-homology (KH0, KH1, and KH2) RNA binding domains and a highly variable (isoform-specific) carboxy (C-) terminal intrinsically disordered region (C-IDR), which in the case of the predominant isoform 1, contains an RNA binding RGG-box. Additionally, the presence of a nuclear localization signal and a nuclear export signal allows FMRP to shuttle between the nucleus and the cytoplasm, with approximately 4% of FMRP detected in the nucleus (6).

It has been previously put forth that FMRP also functions in genome maintenance (7). We recently demonstrated that FXS patient-derived cells accumulate genome-wide DNA double-strand breaks (DSBs), particularly during replication stress (8). We further demonstrated that the DSBs in FXS cells were associated with R-loops (8), which are three-stranded nucleic acid structures formed during transcription when the nascent RNA stably anneals to the template DNA strand, displacing the nontemplate DNA strand (9). R-loops play important roles in gene expression and many biological processes, but they are also an important source of genomic instability, particularly when R-loop formation is exacerbated by replication-transcription conflict (10, 11). Consequently, there are an abundance of cellular proteins that interact with R-loops and promote their resolution. These include helicases that unwind the RNA:DNA hybrids within the R-loop structure, topoisomerases that release the negative supercoil in the DNA duplex behind the transcription machinery, and ribonucleases that degrade the RNA from the RNA:DNA hybrids. In addition, many other regulatory factors have been associated with R-loop metabolism. We previously showed that expression of FMRP, but not the FMRPI304N mutant, ameliorated DSB formation induced by replication-transcription conflict (8). Subsequently, we presented evidence that recombinant FMRP interacts directly with R-loop structures primarily through its C-IDR, making FMRP the archetype of a class of IDR-based

‡ These authors contributed equally to this work.
* For correspondence: Wenyi Feng, fengw@upstate.edu.

R-loop "reader" proteins (12). Our work suggested a genome protective role of FMRP by preventing R-loop accumulation during replication-transcription conflict. This notion is supported by a recent study demonstrating that FMRP preferentially interacts with m5C-modified R-loops and promotes R-loop resolution (13). It was further strengthened by a study demonstrating that FMRP nuclear isoforms colocalizes to mitotic DNA bridges, and the depletion of FMRP nuclear isoforms causes the accumulation of these mitotic bridges, increased DNA damage, and cell death (14). These studies together suggest that FMRP promotes R-loop resolution to prevent DNA damage.

Here, we investigated how FMRP promotes R-loop resolution through the interplay with DHX9, an RNA helicase known to unwind R-loops. DHX9 has been reported to have apparently opposing functions during R-loop regulation. On one hand, DHX9 knockdown HeLa cells showed increased R-loop formation, suggesting that DHX9 prevents R-loop accumulation (15). Consistent with this observation it was recently shown that DHX9 is recruited by the TDRD3/Top3β complex to remove R-loops at specific target genes (16). On the other hand, in cells depleted of the splicing factor proline and glutamine rich RNA splicing protein, the loss of DHX9 led to reduced R-loop levels, suggesting that DHX9 in fact promotes R-loop formation by unwinding dsRNA when RNA splicing is impaired (17). Thus, these studies suggest that DHX9 might prevent or promote R-loop formation in different genetic contexts, making it a challenging but also important target to study the complex nature of R-loop regulation. In the current study, we present evidence that FMRP directly interacts with DHX9 and regulates its helicase activity, subcellular localization, and ultimately chromatin association. We observed that FMRP inhibits DHX9 helicase activity *in vitro* and chromatin R-loop association *in vivo*. These unexpected results led us to propose that the chromatin-bound FMRP serves as a signal, through protein-protein interaction, for both proteins to disengage from the R-loop after DHX9 unwinds the RNA:DNA hybrid. Our study represents a significant advance in the understanding of the mechanisms by which FMRP regulates an R-loop resolution enzyme and promotes genome integrity upon replication stress.

Results

FMRP is enriched in the nucleus and colocalizes with R-loops in response to DNA replication stress in human lymphoblastoid cells

We previously showed that FXS patient-derived cells lacking FMRP have elevated genome-wide DSBs near R-loop forming sites when undergoing replication stress by aphidicolin (APH), a DNA polymerase inhibitor (8). We proposed that FMRP protects the genome by preventing DSBs during induced replication-transcription conflict. Here, we asked whether FMRP alters its expression level and/or its cellular localization in response to APH. The total level of FMRP remained similar with and without APH, with GAPDH and histone H3 serving as cytoplasmic and nuclear controls, respectively (Fig. S1*A*). The nuclear fraction of FMRP approximately doubled in APH treatment compared to dimethyl sulfoxide (DMSO) (vehicle)-treated control (Fig. S1*B*). In contrast, GAPDH and histone H3 maintained their respective localization patterns, with or without APH (Fig. S1*B* and not shown). These results suggest that FMRP has substantial nuclear fraction in human lymphoblastoids, and it becomes further enriched in the nucleus in response to replication stress.

Next, we examined the localization of FMRP relative to R-loops visually. Immunofluorescence microscopy in lymphoblastoid cells revealed a distinct staining pattern of FMRP, which was predominantly distributed in the cytoplasm and at the periphery of the nucleus in DMSO-treated cells (Fig. 1*A*). Upon induction with APH, nuclear levels of FMRP increased (Fig. 1*A*), consistent with the chromatin fractionation experiments. RNA:DNA hybrid signals as observed from S9.6 antibody staining were present in both the cytoplasm and the nucleus, and significantly increased under APH treatment compared to vehicle control (Fig. 1*A*). Importantly, RNase H treatment significantly reduced the RNA:DNA hybrid signals in APH, thus eliminating the difference between the signals in DMSO- and APH-treated samples (Figs. 1*B* and S1*C*). Because S9.6 antibody is known to nonspecifically target dsRNA (18), we also treated the cells with RNase III to remove the spurious signals. Results showed that S9.6 signals were indeed reduced significantly by RNase III treatment; however, the difference between the DMSO- and APH-treated samples persisted (Figs. 1*C* and S1*D*), further supporting that APH-treated samples contained higher level of RNA:DNA hybrids than the DMSO-treated sample. Altogether, these results indicate enhanced R-loop formation with APH, consistent with our previous observation (8). Moreover, quantification of signal colocalization indicated that the percentage of FMRP overlapping with RNA:DNA hybrid signals increases in APH (Fig. 1, *D* and *E*). Notably, this colocalization is reduced in RNase H treatment compared to control but remains unchanged with RNase III, suggesting that FMRP colocalizes with R-loops.

FMRP coimmunoprecipitates (co-IPs) with DHX9 and the I304N mutation abolishes the interaction

We recently showed that FMRP binds R-loop structures directly *in vitro* using electrophoretic mobility shift assay (12). By comparing the dissociation constants between FMRP and individual subcomponents of the R-loop, we proposed a model in which FMRP interacts with the three-way junction of the R-loop primarily through its C-IDR moiety, with the N-Fold likely interacting with the trailing RNA and/or the ssDNA of the R-loop. Because the binding by C-IDR was sensitive to a 5′ ssRNA overhang on the R-loop we surmised that C-IDR binds to the 5′ of the R-loop structure. FMRP lacks apparent protein domains for helicase or nuclease activity. Thus, the ability of FMRP to resolve R-loops must come from its association with its binding proteins. Therefore, we next tested if FMRP interacts with known R-loop-interacting proteins. At the beginning of our study, few FMRP-binding proteins with

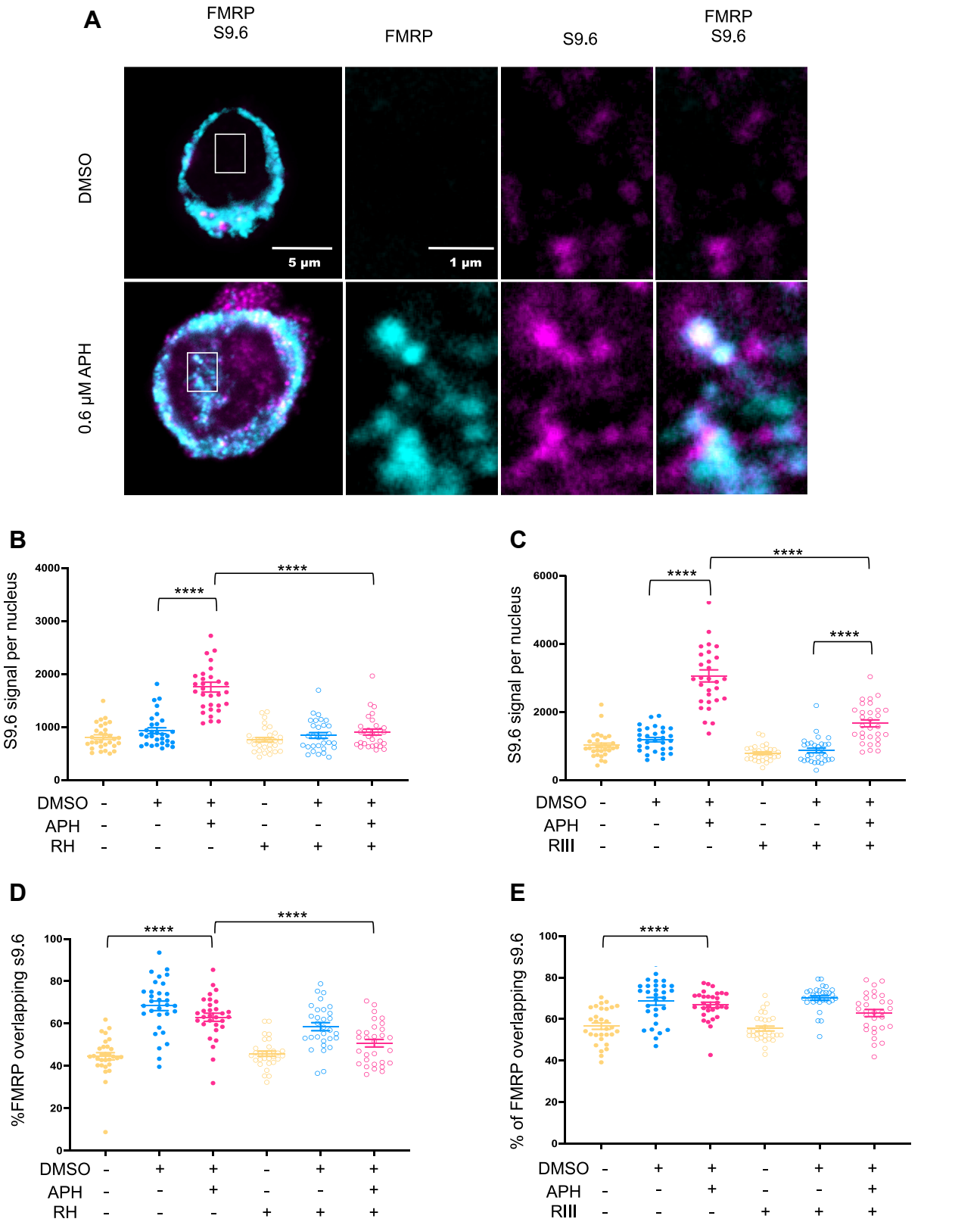

Figure 1. FMRP is enriched in the nucleus upon replication stress and colocalizes with R-loops. *A*, colocalization of FMRP and RNA:DNA hybrids. Immunofluorescence images of DMSO and APH treated GM6990 cells costained for RNA:DNA hybrids (*magenta*), FMRP (*cyan*), and DAPI (*blue*). *B* and *C* quantification of S9.6 signal per nucleus in cells treated with RNase H (*B*) or RNase III (*C*). Error bars indicate standard error of mean (SEM),N∼30 cells. One-way ANOVA followed by Tukey's multiple comparison test, *$p < 0.05$, **$p < 0.01$, ****$p < 0.0001$. *D* and *E*, quantification of colocalization of FMRP with S9.6 signal in experiments with RNase H (*D*) or RNase III (*E*) using Fiji Coloc2 plugin. Error bars indicate SEM,N∼30 cells per sample. One-way ANOVA followed by Tukey's multiple comparison test, *$p < 0.05$, **$p < 0.01$, ****$p < 0.0001$. APH, aphidicolin; DAPI, 4′,6-diamidino-2-phenylindole; DMSO, dimethyl sulfoxide; FMRP, fragile X messenger ribonucleoprotein; RH, RNase H; RIII, RNase III.

functions in the R-loop pathway existed in the literature, so we exploited a large-scale human proteome study and collected all reported interactions with FMRP (19). Both FMRP and DHX9 were pulled down by THOC1, a component of the THO nuclear export complex. Depletion of the THO complex causes DNA damage that is R-loop dependent (20). Therefore, we set out to investigate the potential interaction between FMRP and DHX9. Using the aforementioned GM06990 lymphoblastoids, we first demonstrated coimmunoprecipitation (co-IP) of FMRP and its known interacting protein, FXR1 (FMR1 autosomal homolog 1), as a positive control (21) (Fig. S2*A*). We also detected DHX9 interaction with FMRP through co-IP (Fig. S2*B*). In addition, the complex pulled down by anti-DHX9 also comprised of Top3β (Fig. S2*B*), which has been implicated in R-loop suppression by reducing negatively supercoiled DNA behind RNA polymerase II (22).

We then asked if the *in vivo* FMRP/DHX9 interaction is (i) mediated by nucleic acids and (ii) dependent on the KH2 domain of FMRP. To address these questions, we first generated a CRISPR KO of *FMR1* in HEK293T cells (Fig. 2*A*). We selected a *fmr1* KO (B3 clone) and showed that it recapitulated the DNA damage phenotype of the FXS patient-derived cells we previously described (Fig. 2, *B–D*) (8). We then generated stable cell lines expressing enhanced green fluorescent protein (eGFP)-tagged FMRP and FMRPI304N in the *fmr1* KO cells to facilitate the comparison of WT to mutant FMRP with respect to their interaction with DHX9. The results demonstrated that the *fmr1* KO cells expressing eGFP-FMRP significantly reduced APH-induced DSBs and R-loop formation compared to cells expressing only eGFP, or the mutant eGFP-FMRPI304N (Fig. 2, *E* and *F*). We then carried out reciprocal immunoprecipitations in the *fmr1* KO cells expressing either WT or mutant FMRP. Our results showed that the I304N mutation reduced the interaction between FMRP and DHX9 (Fig. 3, *A* and *B*).

Next, we showed that the FMRP/DHX9 interaction was not mediated by nonspecific association with RNA by comparing the coIP levels with and without RNase A treatment (Fig. S2*C*). In fact, the DHX9 pull-down efficiency from FMRP IP was higher in cells treated with more RNase A, suggesting that nonspecific RNA binding might reduce DHX9/FMRP interaction. Similarly, the interaction between FMRP and DHX9 was not significantly different in cells expressing RNase HI, or a catalytically dead RNase HI, or no expression at all (Fig. 3, *C* and *D*). Expression of RNase HI was verified (Fig. 3*E*). These results led us to conclude that the *in vivo* interaction between FMRP and DHX9 was not dependent on nucleic acids.

FMRP directly interacts with DHX9 in a manner dependent on the KH2 domain

We also sought to determine if FMRP directly interacts with DHX9 using recombinantly purified proteins *in vitro*. Specifically we tested different moieties of the protein (domain structure shown in Fig. S3*A*), including the full length FMRP and portions thereof, the N-terminal folded domain (N-Fold) and the C-IDR, for their ability to interact with DHX9 (Fig. S3, *B*, *D* and *E*). We also generated both the full-length FMRP and the N-Fold containing an I304N substitution (Fig. S3, *C* and *F*), a rare mutation that causes FXS without triplet repeat expansion at the 5′-UTR of *FMR1*. FMRPI304N causes defective RNA binding and polysome association and FXS (23, 24). We previously showed that FMRPI304N has reduced ability to suppress R-loop-induced DSBs during programmed replication-transcription conflict (8). Here, our results showed that recombinant histidine tagged-DHX9 binds directly to recombinant FMRP (Fig. 4*A*). The interaction was relatively weak compared to coIP from cells. We added bezonase in the binding buffer to remove nucleic acids. Therefore, DHX9/FMRP interaction is not mediated by nonspecific binding to nucleic acids. Our results also demonstrated that this interaction was dependent on the N-Fold domain, not the C-IDR, and the I304N mutation in the N-Fold abolished the interaction (Fig. 4, *B* and C). We asked what might the functional importance be for this interaction between FMRP and DHX9. To answer this question we proceeded to test if the FMRPI304N mutation alters chromatin binding by DHX9.

FMRP regulates the chromatin association of DHX9

We first analyzed by chromatin immunoprecipitation coupled with quantitative PCR (ChIP-qPCR) the binding of FMRP or DHX9 at the promoter, intron-5, and the pause site of the β-actin locus, previously shown to form R-loops that interact with DHX9 (15). To our surprise, in cells carrying FMRPI304N (Fig. 5*A*), or lacking FMRP entirely (Fig. S4), DHX9 showed increased presence at the β-actin locus upon treatment with DMSO or APH, compared to cells carrying WT FMRP. This effect was most pronounced in DMSO treatment due to an apparently downregulated chromatin association compared to no treatment in cells expressing WT FMRP. ChIP-seq analysis confirmed these observations genome-wide, comparing the overall binding profile of DHX9 across all genes in cells with WT *versus* mutant FMRP (Fig. 5, *B* and *C*). Interestingly, FMRPI304N also showed higher level of association with the chromatin compared to the WT FMRP, particularly when cells were treated with APH (Fig. 5, *A–C*). These results suggested that abolishing the interaction between FMRP and DHX9 caused both proteins to show elevated levels of chromatin association, presumably with the R-loop. They also suggested that DHX9 chromatin association was negatively correlated with the functional presence of FMRP. Consistent with this notion, we found that exogenously expressed mCherry-DHX9 showed altered subcellular localization in the absence of FMRP. Whereas mCherry-DHX9 showed pan staining pattern in the nucleoplasm in the control *FMR1*$^{+/+}$ cells, its presence in the nucleoplasm appeared to be reduced and instead enriched in the nucleoli of the *fmr1KO* cells (Fig. S5*A*). Moreover, expression of eGFP-FMRP in the *fmr1KO* cells partially reverted this phenotype (Fig. S5*A*). Protein expression was confirmed by Western blot (Fig. S5*B*).

Taking all these results together, there appeared to be an interesting dichotomy between FMRP and DHX9, where DHX9 chromatin association shows negative correlation with the functional presence of FMRP despite their physical

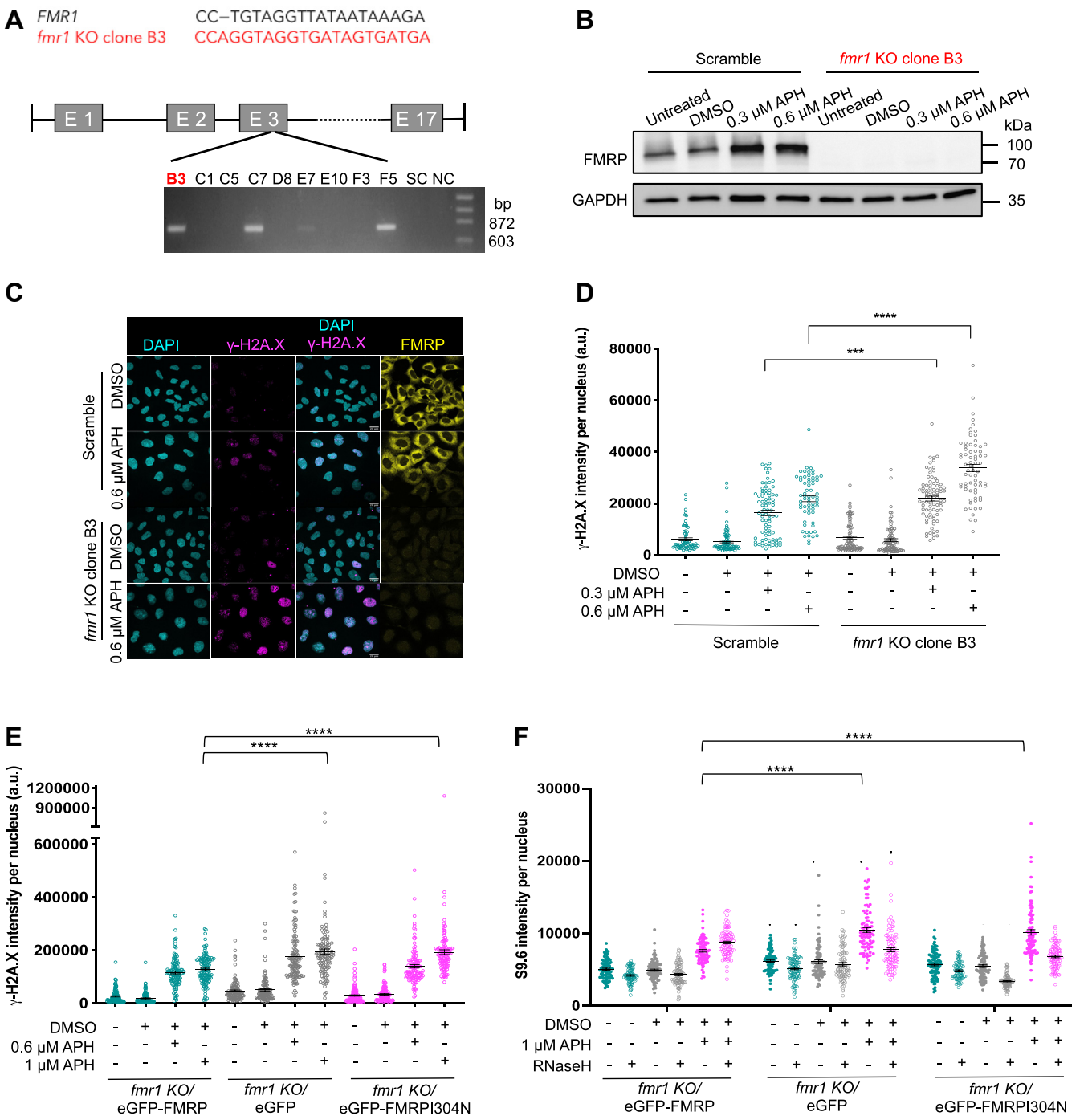

Figure 2. CRISPR KO of *FMR1* gene in HEK293T cells and reexpression of FMRP. *A*, genome structure of *FMR1* with CRISPR target region in exon 3. CRISPR clones analyzed by PCR. Clone B3 is used for all subsequent experiments. "SC", scramble; "NC", no template control. *B*, Western blot confirms the lack of FMRP expression in *fmr1* KO cells. *C* and *D*, increased DNA damage by APH-induced replication stress in *fmr1* KO cells. The scale bar represents 20 μm. N > 60 cells per sample were analyzed. One-way ANOVA test followed by Tukey's multiple testing for all pair-wise comparisons was performed. *E*, retroviral transduction and stable cell line generation of eGFP, eGFP-FMRP and eGFP-FMRPI304N expression in *fmr1* KO cells. DNA damage by APH-induced replication stress after reexpressing FMRP, FMRPI304N or nothing. N > 110 cells per sample were analyzed. One-way ANOVA test followed by Sidak's multiple testing. Two independent experiments were done and a representative experiment is shown for (*D*) and (*E*). *F*, elevated S9.6 in eGFP and eGFP-FMRPI304N expressing *fmr1* KO cells. S9.6 signals were sensitive to RNase H treatment. N > 75 cells were analyzed. Two-way ANOVA test followed by Holm-Sidak's multiple testing. Annotation for *p* values are: *$p < 0.05$; **$p < 0.01$; ***$p < 0.001$; ****$p < 0.0001$. Error bars indicate standard error of mean (SEM). APH, aphidicolin; eGFP, enhanced green fluorescent protein; FMRP, fragile X messenger ribonucleoprotein.

interaction. These results lent to a testable model in which we propose FMRP either blocks (physical sequestration) or disengages DHX9 from the R-loop template. We speculated that DHX9, after unwinding the RNA:DNA duplex and upon reaching the 5′-junction of the R-loop, does not run off the trailing RNA spontaneously as the RNA might be tethered to other binding proteins, and instead requires a signal to disengage from the template. FMRP, by interacting with the

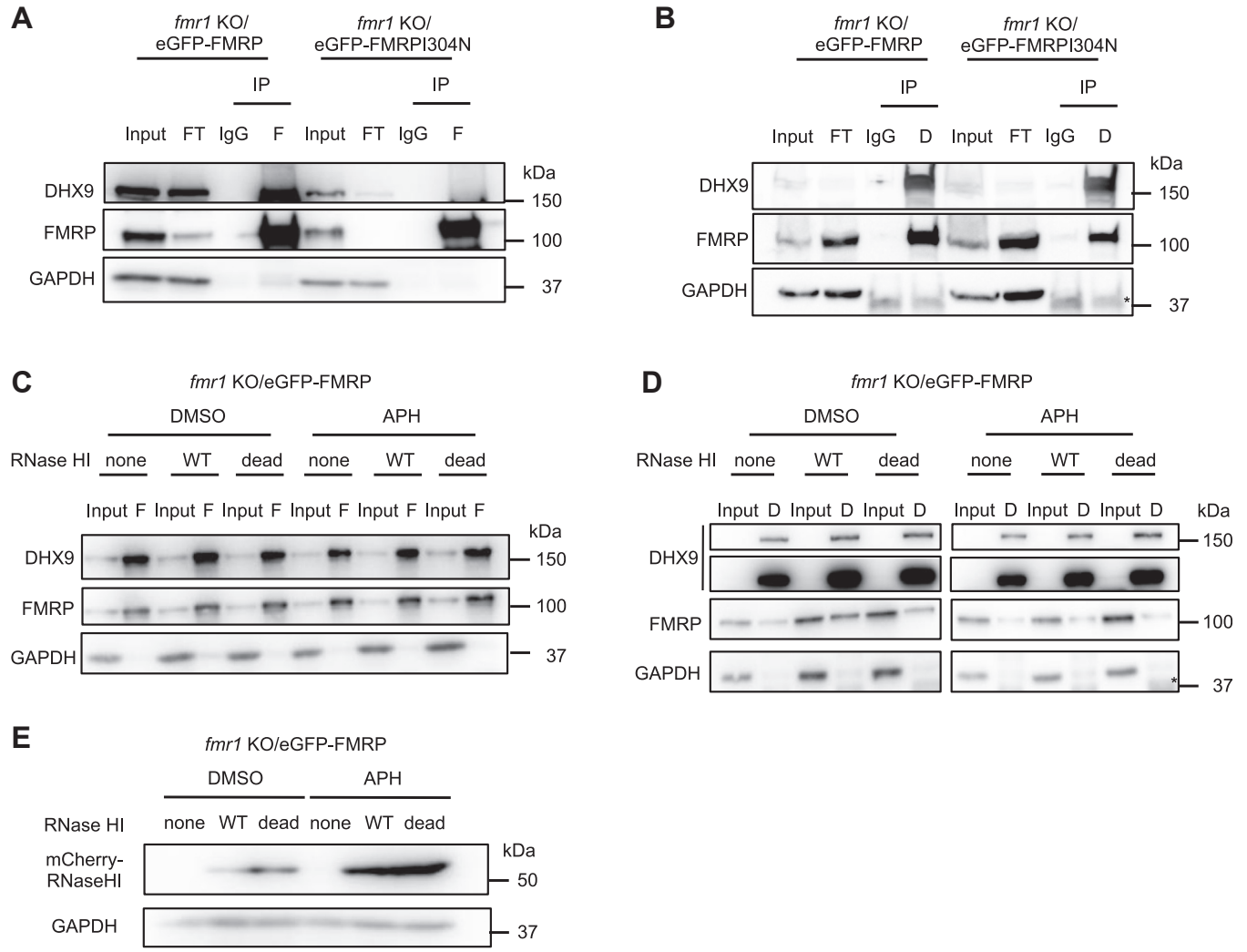

Figure 3. FMRP coimmunoprecipitates (IPs) with DHX9. *A* and *B*, reciprocal IP of FMRP (*A*) and DHX9 (*B*) from *fmr1* KO cells expressing eGFP-tagged FMRP or FMRPI304N. *C* and *D*, reciprocal IP of FMRP (*C*) and DHX9 (*D*) from *fmr1* KO cells expressing eGFP-tagged FMRP or FMRPI304N, and additionally, either WT RNase HI ("WT"), or a catalytically dead RNase HI mutant ("dead"), or the empty vector ("none"). Cells were treated with DMSO, or 1 μM APH. *E*, Western blot showing similar expressions of WT RNase HI and catalytically dead RNase HI mutant tagged with mCherry in the indicated cell lines. APH, aphidicolin; "D", DHX9; DMSO, dimethyl sulfoxide; eGFP, enhanced green fluorescent protein; "F", FMRP; FMRP, fragile X messenger ribonucleoprotein.

three-way junction of the R-loop, may serve as a stop signal for DHX9, possibly by curtailing its helicase activity. This interaction/encounter between the two proteins then leads to dissociation of both proteins from the R-loop. If this model were true, we would make two predictions. First, FMRP would inhibit the helicase activity of DHX9. Second, reducing/abolishing the interaction between FMRP and DHX9 would result in increased dwelling time by DHX9 on the chromatin, thus leading to an increase in colocalization with FMRP. We next tested if FMRP has an impact on DHX9 helicase activity.

FMRP inhibits DHX9 helicase activity on R-loops through its N-Fold domain

DHX9 is a 3′ to 5′ helicase known to be able to unwind dsDNA, dsRNA as well as RNA:DNA hybrid, and in the context of RNA, DHX9 demonstrated a clear preference for the 3′-RNA overhang (25, 26). Therefore, we focused on an R-loop structure with a 3′-RNA overhang, which DHX9 readily unwound and produced free RNA (Fig. 6, *A* and *B*). When presented with increasing concentrations of the N-Fold-WT, the DHX9 helicase activity was steadily reduced, reaching near complete inhibition at 400 nM (Fig. 6*A*). The I304N mutation in the N-Fold reduced the inhibitory effect (Fig. 6*A*). In contrast, the C-IDR did not appear to inhibit DHX9 (Fig. 6*B*). Quantification of % R-loop unwinding from three independent experiments confirmed these observations (Fig. 6*C*). Compared to the separate N-fold, the inhibition by full-length FMRP was less pronounced (Fig. S6, *A* and *B*). This result was consistent with the notion that the N-Fold and C-IDR possess intramolecular interaction *in vitro*, which interferes with the *in vitro* functions of both domains. For instance, we have observed that the C-IDR binds R-loop better than the full-length FMRP (12). Moreover, the I304N mutation, which abolishes the intramolecular interaction, allows the full-length FMRP to bind R-loop equally well as the WT protein (12). Here, we also observed that the I304N mutation had little impact on the inhibitory effect by FMRP

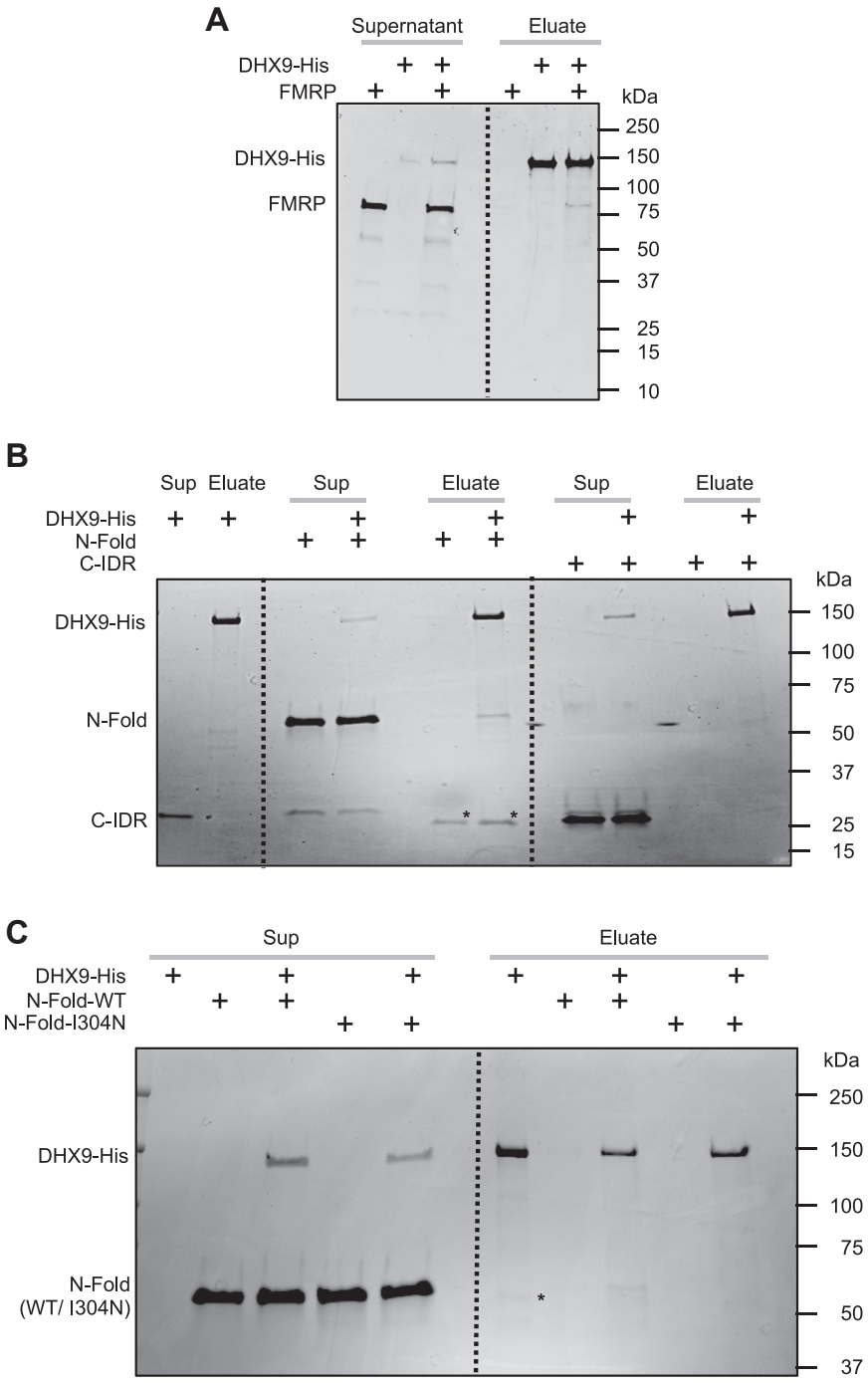

Figure 4. FMRP directly interacts with DHX9. *A–C*, *in vitro* protein binding assays for DHX9-His fusion protein and full length FMRP (*A*), FMRP domains (*B*) and N-Fold-WT or N-Fold-I304N (*C*). Proteins eluted from (Eluate), or flow through (Supernatant or Sup), a Ni-NTA column were analyzed by SDS-PAGE. "*" represents a non-specific band. FMRP, fragile X messenger ribonucleoprotein.

toward DHX9 in the context of full-length FMRP (Fig. S6, *A* and *B*). Therefore, we concluded that FMRP inhibits DHX9 by direct interaction through the N-Fold. Next, we tested the second prediction that FMRP mutant would show increased association with DHX9.

FMRPI304N mutant shows increased colocalization with DHX9

Indeed, cells (a scramble KO control clone) carrying either FMRPI304N or a catalytically dead DHX9 (DHX9-HD, helicase dead) demonstrated more colocalized FMRP and DHX9 (Fig. 7*A*) than the WT counterparts together. This result suggested that the I304N and HD mutations both cause increased dwelling time on the chromatin by DHX9, thereby increasing the probability of colocalization with FMRP. We further tested this hypothesis by performing a proximity ligation assay (PLA) between endogenous DHX9 and WT or mutant FMRP. The results showed that PLA signals were stronger and more enriched in the nucleus in cells expressing the FMRPI304N mutant than those expressing the WT FMRP (Fig. 7, *B* and *C*). Control

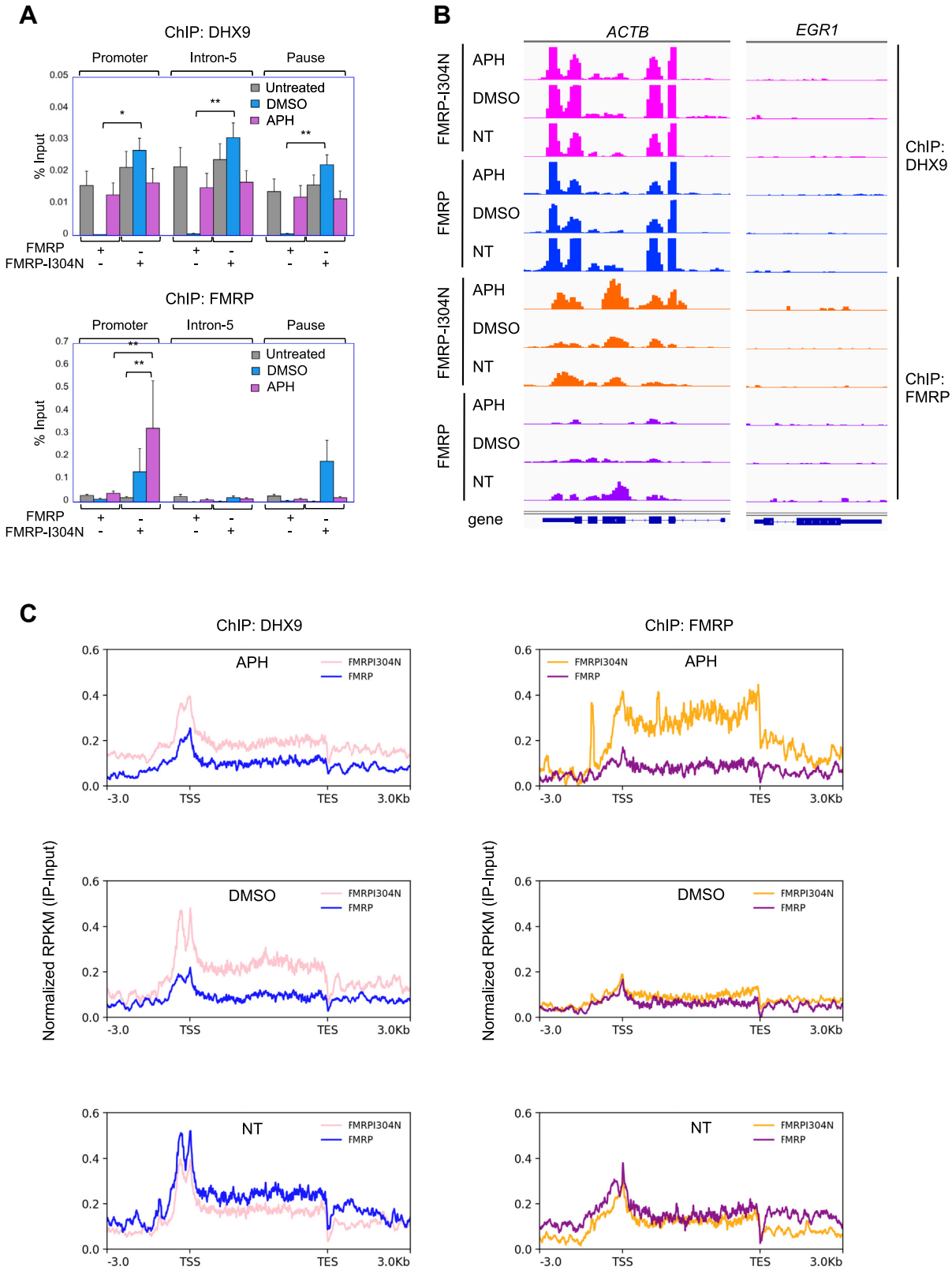

Figure 5. FMRP regulates chromatin association of DHX9. *A*, DHX9 (*top*) or FMRP (*bottom*) ChIP-qPCR across the β-actin locus from *fmr1 KO* cells expressing eGFP-FMRP or GFP-FMRPI304N. Percentage of input was averaged from two independent experiments. *B*, ChIP-seq profiles for the β-actin locus and the early growth response protein 1 negative control locus. *C*, normalized ChIP signals across all genes in cells expressing WT FMRP or FMRPI304N. ChIP-qPCR, chromatin immunoprecipitation coupled with quantitative PCR; eGFP, enhanced green fluorescent protein; FMRP, fragile X messenger ribonucleoprotein; TES, transcription end site; TSS, transcription start site.

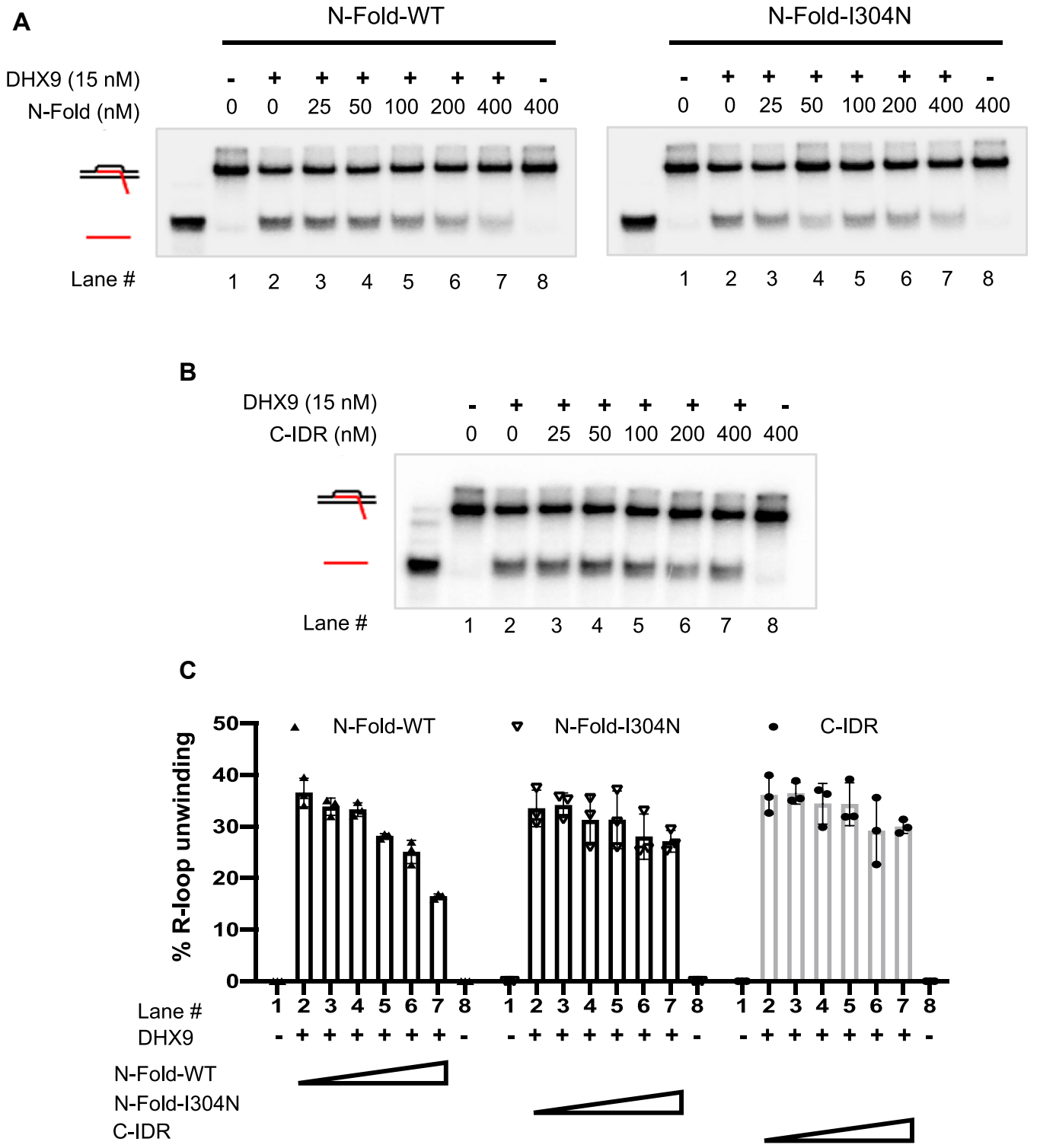

Figure 6. FMRP regulates DHX9 helicase activity. *A*, N-fold of WT FMRP inhibits DHX9 helicase activity more than N-fold-I304N. *B*, C-IDR does not affect DHX9 helicase activity. *Black* strand represents DNA and *red* represents RNA. *C*, quantification of DHX9 helicase activity shown here as percentage R-loop unwinding for N-fold of both WT and mutant FMRP and C-IDR domain. FMRP, fragile X messenger ribonucleoprotein; IDR, intrinsically disordered region.

experiments using only one of the two PLA probes did not show PLA fluorescence (Fig. S7).

Discussion

The work described here was directly predicated on our recent study demonstrating a function of FMRP in preventing replication stress-induced R loop accumulation and DSBs (8). Here, we provided additional support for this genome-protective function of FMRP by demonstrating in a CRISPR KO of *fmr1* model that DNA damage and R-loop formation are both elevated. We further reported that recombinant FMRP directly binds to R-loop structures predominantly *via*

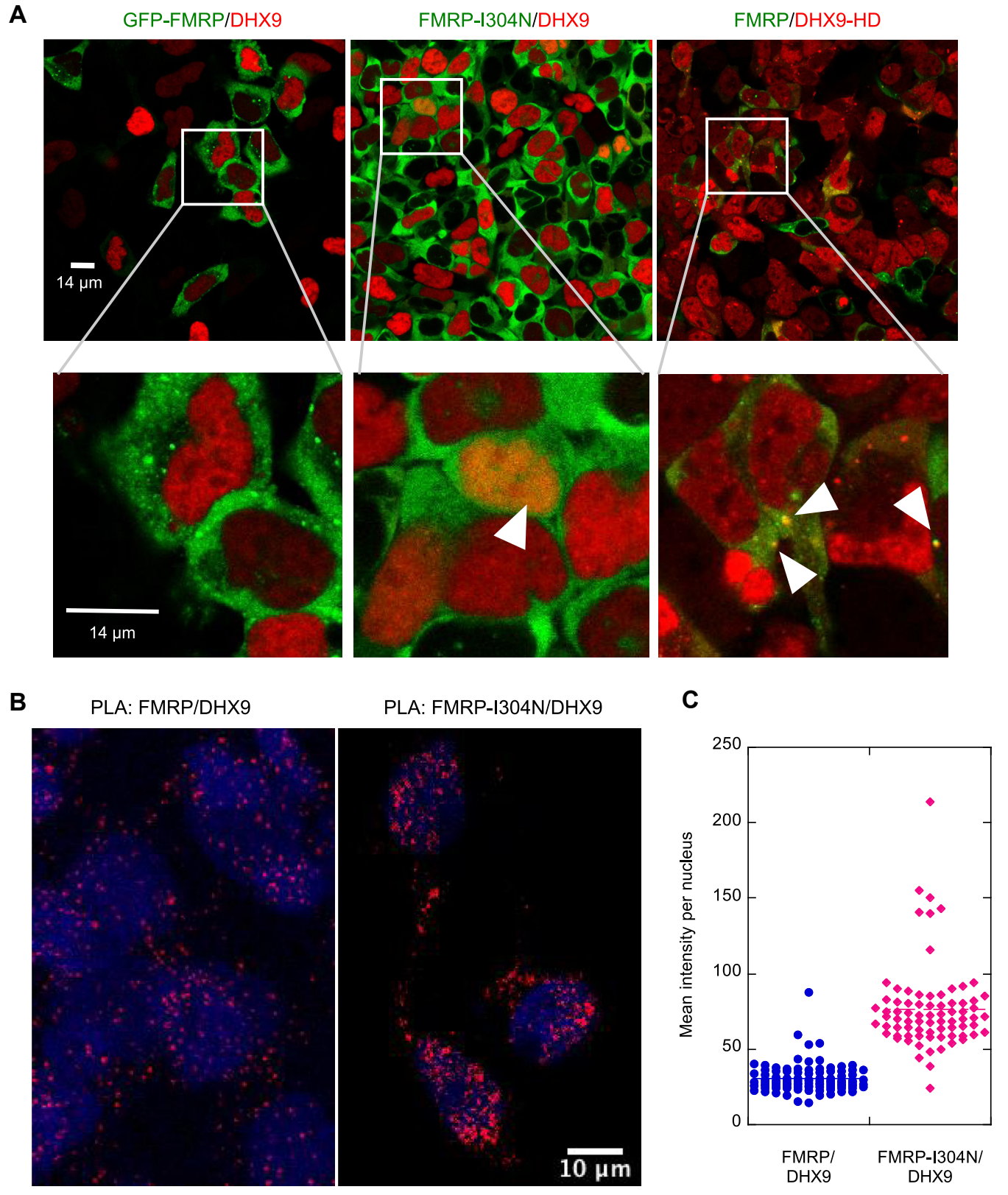

Figure 7. FMRPI304N mutant colocalizes with DHX9 more than WT FMRP. *A*, live cell imaging of scramble KO control cells transiently expressing eGFP-FMRP and mCherry-DHX9, or the mutants thereof. "HD", helicase dead. *B* and *C*, immunostaining for PLA signals in cells expressing the WT FMRP or FMRPI304N. PLA signals were quantified as mean intensity per nucleus (*C*). p = 4.97E-33 by Student's t test with two-tailed distribution and equal variance. eGFP, enhanced green fluorescent protein; FMRP, fragile X messenger ribonucleoprotein; PLA, proximity ligation assay.

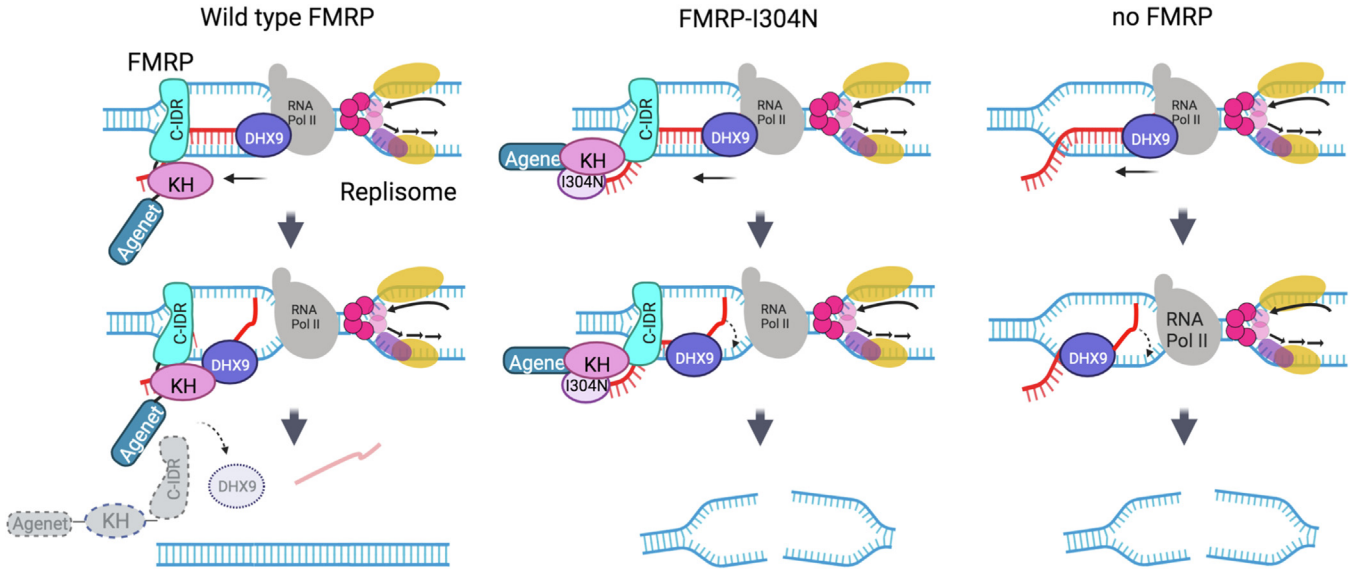

Figure 8. Proposed model for the functional interplay between FMRP and DHX9 at the chromatin. We suggest that FMRP dissociates DHX9 from the chromatin after R-loop unwinding. Cells with either mutant FMRPI304N or no FMRP at all show increased association of DHX9 at the R-loop, allowing R-loop to persist and cause DSBs. FMRP, fragile X messenger ribonucleoprotein.

its C-IDR (12). Based on the hierarchy of substrate binding by the FMRP segments, we propose that, upon replication stress, FMRP binds to R-loops predominantly *via* its C-IDR, thereby allowing the KH domains in the N-Fold to bind the trailing nascent ssRNA or the ssDNA, and the N-terminal Agenet domains to presumably interact with methylated histone tails or R-loop resolving factors that contain motifs with methylated arginine or lysine residues.

Here, we showed that FMRP interacts with one such R-loop resolving factors, DHX9, through its N-Fold domain. Moreover, the interaction is dependent on a *bona fide* KH2 domain, suggesting that mutations in the KH domain may interfere with the Agenet domain's binding to other proteins through disruptions of intramolecular interactions. These results underscore the importance of the KH2 domain in proper FMRP function, and the direct impact on disease manifestation. Moreover, we found that FMRP inhibits the DHX9 helicase activity on R-loops *in vitro*. Consistently, the chromatin association of DHX9 was increased in the absence of a functional FMRP. These results led us to propose a "disengagement" model to describe the complex interplay between FMRP and DHX9 at R-loops (Fig. 8).

We propose that FMRP and DHX9, each capable of binding R-loops directly, are associated with the 5′- and 3′-end of the R-loop, respectively. This mode of interaction is based on the observed substrate preference of FMRP and the known preference of DHX9 for substrates with a 3′-overhang and its association with RNA Pol II. Once engaged on the 3′end of the RNA, DHX9 unwinds the DNA:RNA hybrid within the R-loop toward the 5′ end. We note that very little is known about how DNA translocases disengage from the *in vivo* substrates, a problem that likely does not exist in *in vitro* assays as the substrate has finite length and is not tethered to the chromatin. Therefore, we propose that once poised at the 5′ end three-way junction of the R-loop, FMRP functions as a signal for DHX9 to stop translocation and disengage from the chromatin upon completion of unwinding the DNA:RNA hybrid. We further posit that this interaction also leads to the disengagement of FMRP from the chromatin. The underlying basis for this disengagement may very well come from DHX9 itself *via* its ATPase activity, as DExD/H box RNA helicases are known to regulate the dissociation of other proteins (27). In the absence of a functional FMRP, such as in the FMRPI304N mutant, FMRP fails to interact with DHX9 and both proteins persist, thus allowing the RNA strand to reenter to form the R-loop, ultimately causing DSBs. We predict that in the absence of FMRP such as in the FXS patients, DHX9 would also persist on the chromatin, thus equally permissible for the R-loop to reform.

However, we note that a competing "blockage" model must also be entertained (not depicted). It has been suggested that in certain genetic background such as splicing mutations, DHX9 promotes R-loop formation by unwinding the secondary structure in the RNA transcript and permitting its reentry into the DNA template to form hybrids (28). It is possible that FMRP actively curtails the helicase activity of DHX9 on dsRNA and thereby prevents R-loop formation. We have used an *in vitro* assay with radioactively labeled dsRNA and cold DNA bubble to measure R-loop formation after DHX9 unwinds the dsRNA to allow it to enter the DNA bubble. Thus far, we have not observed any evidence of FMRP having an impact on this activity of DHX9 (data not shown). However, we note that the *in vitro* dsRNA substrate is not a preferred substrate for FMRP, which might mask the potential impact by FMRP on the DHX9 helicase activity on dsRNA. Additionally, when evaluating the impact of this "disengagement" model for the DHX9-FMRP interplay, we must also consider the fact that FMRP interacts with numerous proteins, though predominantly cytoplasmic proteins. It is conceivable that FMRP also regulates other R-loop enzymes, where it assumes a different role than it does in the context of DHX9. A recent human interactome analysis in

HeLa cells revealed an interaction between FMRP and the THO/TREX complex, which functions at the interface of transcription elongation and mRNA export (19). THOC1, a subunit of the THO/TREX complex was present in the same complex as FMR1, DHX9, and other THOC proteins. Depletion of subunits in the hTHO complex causes DNA damage that is R-loop dependent (20). Our coimmunoprecipitation experiments also showed an interaction between FMRP and TOP3B, whose loss causes R-loop-mediated genome instability (29). This result suggests that FMRP forms multiple docking sites for factors that resolve R-loops and ensures proper transcription, RNA processing, and export.

Finally as a closing thought, modular proteins such as FMRP and DHX9, which contain multiple folded domains interspersed with intrinsically disordered regions, often undergo liquid-liquid phase separation, where molecules spontaneously demix from their solvent to form their own microscopic droplets (30–32). The C-IDR of FMRP is capable of undergoing phase separation in isolation, in the context of full length, and in the presence of its cognate RNA substrates (33). The multivalent interactions between FMRP segments, R-loop substructures and R-loop resolving factors (*e.g.*, DHX9) can be the basis for the assembly of a phase-separated, membrane-less foci for resolving R-loops (12).

Experimental procedures

Cell lines and culture conditions

Human EBV transformed lymphoblastoid cell lines, GM06990 (control) and GM03200 (Fragile X) were obtained from Coriell institute. Lymphoblastoids were grown in RPMI1640 (Corning), supplemented with GlutaMAX (GIBCO), 15% heat-inactivated fetal bovine serum (FBS, Benchmark), 100 IU/ml penicillin and 100 μg/ml streptomycin (Corning) at 37 °C with 5% CO_2. HEK293T (American Type Culture Collection (ATCC) #ACS-4500) cells and Phoenix-AMPHO producer cells (ATCC #CRL-3213) were grown in Dulbecco's modified Eagle's medium (Gibco) supplemented with 10% FBS, 1X GlutaMAX, 100 IU/ml penicillin and 100 μg/ml streptomycin, 1 mM sodium pyruvate (Corning), 10 mM Hepes buffer (Corning) and 1X minimum essential medium nonessential amino acids (Corning) and grown at 37 °C with 5% CO_2.

Generation of CRISPR KO of FMR1

FMR1 sgRNA CRISPR/Cas9 All-in-One Non-viral Vector set (Human) (abm # K0790727) containing three targets (T1, T2, and T3) were used to create *FMR1* KO lines in HEK293T cells. Additionally, CRISPR Scrambled sgRNA All-in-One Non-Viral Vector (with spCas9) (abm #K094) was used as control for the KO. HEK293T cells were seeded onto 60 mm plates at 80% confluency and transfected using DNAfectin Plus Transfection reagent (abm) following manufacturer's instruction. Briefly, 5 μg of each construct (Scr, T1, T2 and T3) was mixed with serum-free and antibiotic free media. Fifteen microliters of the transfection reagent was added to this mixture and incubated for 30 m in room temperature. Following incubation, the mixture was added drop-wise to the cells after 20 h of seeding. Forty-eight hour post transfection, cells were trypsinized, washed, and resuspended in fluorescence-activated cell sorting buffer (2% FBS in 1X PBS) and filtered through filter-topped flow tubes (BD falcon) using a luer-lock syringe at 2 × 10^6 cells/ml. Cells were sorted and selected for mid-intensity GFP signal using untransfected cells as a control. Single cells were seeded on to 96-well plate containing media for generating clones for all targets and the scramble. 10 to 11 clones per target and scramble were further expanded for Western blot analysis of FMRP expression. Ultimately, 3 to 5 clones per target showing optimal loss of FMRP expression (no visible FMRP expression) was selected for further analysis. Genomic DNA was isolated from these clones using CRISPR genomic cleavage detection kit (abm) and PCR amplification of sequences around the target region using primers; FMR1_T1_F: 5′-CTCAGCTCCGTTTCGGTTT-3′, FMR1_T1_R: 5′-AAAGGGGGAATAAGCCATCG-3′, FMR1_T2_F: 5′-ATTGCCGTTATGTCCCACTC-3′, FMR1_T2_R: 5′-TCAACGGGAGATAAGCAGGT-3′, FMR1_T3_F: 5′-CTGCCTACCTCGGGGTACAT-3′, FMR1_T3_R: 5′-GCTCTTGCAAACCAAACCAT-3′, was conducted. The PCR product was then sequenced and the sequences were analyzed to verify substitution, addition or deletion of nucleotides at the target region indicating a mutation and leading to loss of FMRP expression. B3 clone of Target-3 was used for the rest of the experiments and for generation of EGFP alone, EGFP-FMRP and EGFP-FMRPI304N fusion protein expressing stable cell lines.

Generation of EGFP-fusion protein stable cell lines

Plasmids expressing FMRP and FMRPI304N was generated as described previously (8). mCherry was PCR amplified from mCherry-Alpha-5-Integrin-12 (Addgene #54970) using forward primer 54970RMmCherryaddNHis_F2: 5′-CGAGGTTAACATGGGCCATCATCATCATCATCATATGGTGAGCAA-3′, and reverse primer, 54970RMmcherry_R1: 5′-CCATGAATTCCTTGTACAGCTCGTCCATGCCGCCG-3′, cloned into pMSCVpuro (Addgene #K1062-1) at Hpa1 and EcoR1 sites to create pMSCVpuro-His-mCherry. DHX9 and DHX9 helicase dead mutant (DHX9-HD) were PCR amplified from pFBDual-DHX9 and pFBDual-DHX9 helicase dead mutant (gifts from Sung lab), using forward primer pFB_rmdhx9+N3AAs_F2: 5′-ACCCGAATTCAACTTGGTTATGGGTGACGTTAAAAATTTTCTG-3′, and reverse primer, pFB_RMDHX9_R1: 5′-GGTAGAATTCTTAATAGCCGCCACCTCCTCTTCC-3′, and cloned to pMSCVpuro-His-mCherry at EcoR1 site to create pMSCVpuro-His-mCherry-DHX9 and pMSCVpuro-His-mCherry-DHX9-HD. These constructs were then packaged into retrovirus using Phoenix-AMPHO producer cells (ATCC #CRL-3213) as described previously (8). Viral particles so generated were then used to transduce *fmr1* KO-clone B3 or Scramble cells and generate pooled population of eGFP-FMRP, eGFP-FMRPI304N, eGFP alone and maintained in 0.25 μg/ml puromycin containing media. Cells were sorted and selected for mid-intensity GFP signal using the parent *fmr1* KO-clone B3 cells as a control. eGFP expressing single cells were seeded on to

96-well plate containing media for generating clones for all cell lines. Pooled cells expressing both eGFP and mCherry signals were selected with fluorescence-activated cell sorting. Protein expression was verified by microscopy and Western blot.

RNase HI overexpression

pICE-RNaseHI-NLS-mCherry (Addgene #60365), or pICE-RNaseHI-D10R-E48R-NLS-mCherry (Addgene #60367), or an empty vector without RNase HI was transfected into FMR1KO-B3-FMRP-H9 and FMR1KO-B3-FMRPI304N-F10 cells using TransIT-2020 transfection reagent (Mirus Bio) following manufacturer's instruction. The empty vector was subcloned by blunt end ligation of a *Hind* III/*Sbf* I digestion. Twenty-four hours after transfection, cells were treated with DMSO and APH separately or left untreated. Forty-eight hours after transfection lysates were prepared for co-IP as described above.

Recombinant protein purification

As previously outlined by Tsang *et al* (33) and briefly described here, codon optimized full length human FMRP Isoform 1 complementary DNA was generated by gene synthesis (GeneScript, Inc) and was subcloned into a pET-SUMO vector (Invitrogen). This pET-SUMO-FMRP plasmid was used as a template to generate (i) full-length I304N mutant, (ii) FMRP-WT and FMRPI304N mutant N-Folds (residues 1–455 without and with the I304N substitution, respectively), and (iii) C-IDR (residues 445–632) *via* QuikChange Site-Directed Mutagenesis (Agilent) for protein expression. The fidelity of these constructs was confirmed by Sanger sequencing (Eurofins Genomics). Each construct was transformed into *Escherichia coli* BL21(DE3) Codon Plus Cells (Agilent). Select colonies were inoculated in 50 ml of LB medium, before dilution into 1 L fresh LB medium in a Fernbach flask and grown at 37 °C. Protein expression was induced with 1 mM IPTG at an absorbance (600 nm) of ∼0.6 and was incubated at 16 °C for 18 h. Cells were harvested by centrifugation at 15,000 rpm for 30 m. The supernatant was carefully discarded, and each cell pellet was stored at −20 °C until ready for protein purification.

To begin purification, frozen cell pellets were thawed and resuspended in 100 ml of lysis buffer containing 100 mM NaCl, 50 mM Na_2PO_4, 200 mM arginine HCl, 200 mM glutamic acid, 10% glycerol, 10 mM β-mercaptoethanol, and 1% Chaps, pH 7.4, supplemented with DNase I, lysozyme, and protease inhibitors (bestatin, pepstatin, and leupeptin). Cells were lysed by sonication and the lysate was subjected to centrifugation at 15,000 rpm for 30 m. The supernatant was loaded onto a 20 ml HisTrap HP column (GE HealthCare) equilibrated in the binding buffer (*i.e.* same composition as lysis buffer, but without DNase I and lysozyme) and incubated at 4 °C for 30 m. The column was extensively washed three times with 30 ml of the equilibration buffer. SUMO-fusion proteins were eluted using the same equilibration buffer supplemented with 500 mM imidazole, and fractions containing proteins were combined. A 6X-His-tagged Ulp protease was added to cleave the His-SUMO tag at room temperature overnight with rocking. Completion of the Ulp cleavage reaction was confirmed by SDS-PAGE. After cleavage, the protein solution was passed through a 0.2 μm filter to remove any aggregated product, before it was concentrated using a 5 kDa-cutoff Amicon concentrator by centrifugation at 4000 rpm at room temperature. The concentrated protein solution is again filtered before being loaded onto an equilibrated Superdex 200 size exclusion column (GE HealthCare) to separate the FMRP constructs from the Ulp protease and the His-SUMO fusion tag. Fractions containing pure FMRP proteins were identified by SDS-PAGE and combined for storage at −80 °C.

Recombinant DHX9-His was generated with modifications to a method reported previously (28). DHX9-His was expressed by transducing 800 ml Tni cell culture in ESF921 serum-free media (Expression Systems) at a density of 1×10^6 cells/ml with 16 ml baculoviral suspension (generated in Sf9 cells) and grown for 70 h at 27 °C with shaking. Cell pellet was resuspended in a lysis buffer containing 50 mM Tris–HCl, pH 7.5, 500 mM KCl, 10% glycerol, 1 mM EDTA, 1 mM DTT, 0.01% NP-40, 2 mM ATP, 4 mM $MgCl_2$, 10 mM imidazole, complete protease inhibitor cocktail (MilliporeSigma), and 1 mM PMSF, with sonication. The lysate was clarified by ultracentrifugation at 40,000 rpm for 45 m. The clarified lysate was incubated with 1 ml Ni-NTA resin (Qiagen) for 1 h, followed by washing the resin with 400 ml wash buffer-A containing 50 mM Tris–HCl, pH 7.5, 1000 mM KCl, 10% glycerol, 1 mM EDTA, 1 mM DTT, 0.01% NP-40, 4 mM ATP, 8 mM $MgCl_2$ and 20 mM imidazole. Protein-bound resin was washed again with 50 ml wash buffer-B containing 50 mM Tris–HCl, pH 7.5, 100 mM KCl, 10% glycerol, 1 mM EDTA, 1 mM DTT, 0.01% NP-40, and 20 mM imidazole, followed by elution with 10 ml elution buffer containing 50 mM Tris–HCl, pH 7.5, 100 mM KCl, 10% glycerol, 1 mM EDTA, 1 mM DTT, 0.01% NP-40, 300 mM imidazole and cOmplete protease inhibitor cocktail (MilliporeSigma). The elution was subjected to ion exchange purification with equilibrated Hitrap SP HP (1 ml) column at a gradient of 100 to 500 mM KCl. The peak fractions containing the protein were pooled together and purified again with HitrapQ (1 ml) column. The peak fraction was aliquoted, flash frozen with liquid nitrogen, and stored at −80 °C. The protein was also evaluated *via* size exclusion chromatography by loading 400 μl of the Hitrap SP HP purified fraction onto Superdex 200 increase 10/300 Gl column (GE HealthCare), and a monodisperse peak was obtained at 11.8 ml elution fraction.

Immunocytochemistry and microscopy

Lymphoblastoid cells

Approximately 4×10^5 lymphoblastoid cells after 24 h drug treatment described in the main text were pelleted, washed, and resuspended in 500 μl 1X PBS. Cells were seeded onto 0.5 μg/ml poly-D-lysine (Sigma-Aldrich) coated coverslips in a 24-well plate. Cells were allowed to adhere for 5 m. A total of 125 μl of 4% paraformaldehyde was used to spike the cells for 2 m at room temperature, followed by removal of the solution and replaced by fresh 500 μl 4% paraformaldehyde. Cells were

washed three times with 1X PBS and permeabilized for 30 m with permeabilization buffer (0.5% Triton-X in 1X PBS). Following permeabilization, cells were subjected to RNase H (15 U/well) or RNase H (New England Biolab) buffer only treatment for 4 h and RNase III or RNase III buffer (Ambion, Invitrogen) only for 30 m at 37 °C. Enzyme treatment was followed with two washes with 1X PBS. *HEK293T cells*: 5 × 10^4 cells were seeded onto 0.1 mg/ml coated poly-D-lysine coverslips in a 24-well plate and cultured for 36 h. At 70% confluency, cells were treated with drugs for 24 h. Post treatment, cells were fixed with 500 µl 2% paraformaldehyde for 20 m at room temperature followed by gentle washing with PBS three times. Cells were then blocked with 500 µl PBSAT (1% bovine serum albumin (BSA), 0.5% Triton X in PBS) for 1 h at room temperature. Fifty microliters of primary antibody solution was applied to all coverslips and incubated overnight at 4 °C, washed with PBSAT, and incubated with 50 µl secondary antibody for 1 h at room temperature. Cells were then washed with PBSAT followed by PBS and mounted on glass slides using mounting media (Prolong Diamond antifade plus 4′,6-diamidino-2-phenylindole (DAPI), Invitrogen). Coverslips were allowed to solidify for 24 h before imaging on Leica SP8 confocal fluorescence microscope. Antibodies used for immunostaining include the following: primary antibodies: anti-γH2A.X, Cell Signaling #9718S, 1:400, anti-FMRP, Cell signaling/Biolegend, 1:200; S9.6, Kerafast #ENH001, 1:250; anti-LaminA+C, Novus Biologicals # NBP2-25152, 1:500, and secondary antibodies: Alexa fluor 488, 568, and 647, Invitrogen # A-21206, A10037 and A-21449, respectively, 1:400. To determine localization of FMRP and R-loop in the nucleus, single plane images were obtained. For measurement of S9.6 signal, a region of interest (ROI) in unperturbed images of DAPI was used, which was overlaid on S9.6 signal and Fiji (https://imagej.net/software/fiji/) was used to measure integrated density of the ROI. For measuring colocalization, Coloc2 plugin in Fiji was used with DAPI as ROI. Manders's overlap coefficient was calculated for both the channels and tM1; FMRP's overlap with RNA:DNA hybrids was used to calculate percentage overlap. For the purpose of presentation, images were adjusted for background and contrast and smoothed using a gaussian blur of 1 in Fiji and representative images were used. To quantify DNA damage, γH2A.X signal in nucleus was measured from single plane images. A ROI in unperturbed images of DAPI was used and overlaid on γH2A.X signal. Fiji was used to measure integrated density of the ROI.

Live-cell experiments and imaging

Stably transfected cells coexpressing EGFP-FMRP and mCherry-DHX9, or EGFP-FMRP and mCherry-DHX9-HD were grown at 37 °C (5% CO_2) in Dulbecco's modified Eagle's medium (Gibco) supplemented with 10% FBS (Benchmark). Cells were plated and cultured in 12-well glass bottom plates (Cellvis) before live-cell imaging. Images were taken on a Leica stimulated emission depletion (STED) 3X nanoscope with a 93X glycerol objective.

Proximity ligation assay

PLA was performed with the Duolink *In Situ* Fluorescence Kit (Sigma-Aldrich) according to the manufacturer's instructions except Wash A and B buffers were substituted for PBSAT (PBS, 1% BSA, 0.5% Triton-X) and PBS, respectively. Cell seeding, fixing, and primary antibody incubation conditions were as described above except ∼2 × 10^4 cells were seeded per well in a 24-well plate. Mouse anti-FMRP (Biolegend) and rabbit anti-DHX9 (Bethyl laboratories) were used at 1:200 and 1:100, respectively. Images were collected on Leica SP8 confocal fluorescence microscope. Z-stack images were processed by maximum projection and then used to quantify the PLA signals in nuclei. All image processing was performed with Fiji.

Co-immunoprecipitation

Approximately 6 to 7 × 10^6 cells were used for each IP reaction. Cells were resuspended in 1 ml IP lysis buffer [25 mM Tris–HCl pH 7.5/150 mM NaCl/1% NP-40/1 mM EDTA/5% glycerol/Halt protease inhibitor cocktail (Thermo Fisher Scientific)/Halt phosphatase inhibitor cocktail (Thermo Fisher Scientific)] and incubated on ice for 1 h. Cell lysates were sonicated to fragment the chromatin and reduce viscosity followed by centrifuged at 10,000 rpm for 10 m. Protein concentration in the supernatant was determined using Pierce protein assay reagent (Thermo Fisher Scientific). Fifty microliters of Dynabeads protein G (Invitrogen) per reaction was incubated with 200 µl antibody binding buffer [1X PBS/0.02% Tween 20] and 5 µg of anti-FMRP (Biolegend) and anti-FXR1(Santa Cruz Biotechnology #sc-374148), or 4 µg anti-DHX9 (Santa Cruz Biotechnology #sc-137232), 5 µg mouse immunoglobulin G (IgG) control (Biolegend) or 4 µg rabbit IgG (Bethyl laboratories) in a rotator for 10 m at room temperature. The immunocomplex was rinsed with 200 µl antibody binding buffer at room temperature, followed by incubation with 500 µg of cell lysate per reaction at 4 °C overnight. After incubation the supernatant was saved as flow-through and the beads were washed twice with IP lysis buffer without NP-40. Fifty microliters 2X Laemmli buffer was added to the beads and boiled for elution, before analysis on 8% SDS-PAGE or gradient (4–15%, Bio-Rad) gels and Western blotting using anti-FMRP (Cell signaling #LS-C82231, 1:500 or Biolegend #6B8, 1:1000), anti-GAPDH (Santa Cruz Biotechnology #sc-47724, 1:4000) or anti-DHX9 (Santa Cruz Biotechnology #sc-137232, 1:500), anti-Top3β (Santa Cruz Biotechnology #sc-137238, 1:1000) anti-FXR1 (Santa Cruz Biotechnology, 1:1000), anti-GFP (Santa Cruz Biotechnology #sc-9996, 1:1000) and anti-mCherry (Santa Cruz Biotechnology #sc-390909, 1:100). For RNase A treatment experiments, lysates were first divided into equal protein aliquots and treated with multiple concentrations (as shown in figure) of RNase A or left untreated for 20 m on ice. These lysates were then used for IP as described above.

Chromatin immunoprecipitation (ChIP)

Cell collection

FMR1KO-B3-eGFP, FMR1KO-B3-eGFP-FMRP-H9, and FMR1KO-B3-eGFP-FMRPI304N-F10 cells were grown to 75%

confluency, then treated with DMSO/APH or left untreated for 24 h. Cells were fixed and harvested using the truChIP chromatin shearing kit (Covaris), and IP was conducted according to Richard Myers lab ChIP-seq protocol. Briefly, cells were first washed with room temperature 1X PBS. Then, 5 ml fixing buffer A was added, followed by addition of formaldehyde (methanol-free) to 1%, and then incubated for 10 m at room temperature. To stop the reaction, 300 μl of quenching buffer was added and incubated for 5 m. Cells were collected by scraping (one confluent 150 mm plate per reaction), flash frozen in liquid nitrogen, and stored at −70 °C. Cells were thawed on ice with 1 ml of 1× lysis buffer B and Halt protease inhibitor cocktail (Thermo Fisher Scientific) and incubated with agitation for 10 m. Nuclei were prepared by centrifuging the lysate at 1700*g* for 5 m. The nuclear pellet was washed with 1× wash buffer C and then once with shearing buffer D3 with Halt protease inhibitor cocktail (Thermo Fisher Scientific). Nuclear pellet was then resuspended in 900 μl shearing buffer D3 and sonicated in Covaris M220 ultrasonicator using the protocol 'ChIP_10%df_10 min' (75 W peak power, cycle per burst: 200, duty factor: 10, time: 600 s). The sonicated mixture was centrifuged at 13,500 rpm for 15 m at 4 °C. The supernatant was adjusted to 150 mM NaCl, 10 mM Tris–HCl pH 7.5, 1% NP-40, 0.5% sodium deoxycholate. Approximately 5 to 11% of this nuclear preparation was set aside as "input". The rest was used for immunoprecipitation. Both aliquots were snap frozen in liquid nitrogen and stored at −70 °C.

Immunoprecipitation

A total of 300 μl M280 Dyna beads sheep anti-rabbit IgG (Life technologies) was added to 1 ml freshly prepared PBS with 5 mg/ml BSA (PBS/BSA) and Halt protease inhibitor cocktail (1X). The magnetic beads were washed 3 times in PBS/BSA. Twelve micrograms of monoclonal anti-DHX9 (Bethyl Laboratories) or 5 μg of monoclonal anti-FMRP (Biolegend) was mixed with the beads in 1 ml PBS/BSA and incubated overnight at 4 °C with agitation. The antibody-conjugated beads were washed three times with PBS/BSA, and the nuclear preparation was thawed and added to the beads, followed by incubation at 4 °C with rotation overnight. The beads were washed 5 times with cold LiCl wash buffer (100 mM Tris pH 7.5, 500 mM LiCl, 1% NP-40, 1% sodium deoxycholate), and once with TE buffer (10 mM Tris-HCl pH 7.5, 0.1 mM EDTA). Two hundred microliters of IP elution buffer (1% SDS, 0.1 M $NaHCO_3$) was added to the beads, mixed, and incubated at 65 °C for 2 h with vortex every 30 m. The "input" was thawed and together with the supernatant from the IP sample was reverse-cross-linked at 65 °C overnight. Samples were then treated with 60 μg of proteinase K for 1 h at 55 °C. DNA was purified using Qiagen PCR purification kit and used for qPCR.

Quantitative real-time PCR (qPCR)

After IP and DNA isolation, the ChIP DNA and the input DNA were diluted in H_2O. The PCR reaction was carried out in 10 μl with 5 μl of 2X iTaq Universal Sybergreen Supermix (Bio-Rad), 500 nM of forward and reverse primers to amplify the β-actin locus at the promoter, intron-5 and pause sites (15), and 3 μl of template DNA. PCR conditions were as described (34). Briefly, CFX Opus 384 real time PCR system (Bio-Rad) was used for qPCR with the following thermal cycling protocol: one cycle of 95 °C for 30 s; 39 cycles of 95 °C for 10 s and 60 °C for 30 s; followed by melt curve analysis from 65 °C to 95 °C by an increment of 0.5 °C for 5 s. qPCR data was analyzed and "% Input" was calculated as described (34).

ChIP-seq

Chromatin IP was performed similarly as described above with some modifications. Briefly, 20 million cells were used for each ChIP reaction. Cells were cross-linked by 0.5% formaldehyde, 10 mM NaCl, 0.1 mM EDTA, 0.5 mM EGTA, 5 mM Hepes buffer, pH 8.0 instead of 1% formaldehyde. Cell lysis was performed with 1X lysis buffer B as above, except the lysate was passaged through a 21 g needle 6 times. Additionally, 0.5% SDS and 1% NP-40 was added to the nuclear extract, followed by passaging through a 21 g needle 6 times, before sonication. Sonication was performed with the same protocol above except with 20 m instead of 10 m. The supernatant from the nuclear extract was adjusted to contain 150 mM NaCl before IP. Both input control and IP samples were used for standard Illumina TruSeq library construction, followed by multiplexed sequencing on a HiSeq 2500 platform. Sequence reads were mapped and filtered by Bowtie2 as previously described for Break-seq libraries (8). Mapped reads were then normalized to reads per kilobase per million (RPKM), followed by normalization to input controls by subtraction using deepTools bamCompare (35).

Subcellular fractionation

Cells were grown to a density of 0.4 to 0.5 × 10^6 cells/ml with >90% viability. Cells were treated for 24 h with APH, DMSO, or nothing. Samples were collected as aliquots of approximately 5 × 10^6 cells, washed twice with PBS, and then frozen for storage. Each thawed aliquot of cells was resuspended in 500 μl Farnham's lysis buffer without NP-40 [5 mM Pipes pH 8.0/85 mM KCl/Halt protease inhibitor cocktail] and incubated on ice for 2 m. Fifty microliters of the cell lysate thus prepared was collected as a whole cell extract control, and the remaining lysate was spun at 1300 g for 4 m to pellet nuclei. The supernatant served as the crude cytoplasmic fraction. The nuclear pellet was resuspended in 150 μl Farnham's lysis buffer and incubated for 20 to 30 m at 4 °C and served as the nuclear fraction. Equal volume of 2X Laemmli buffer was added, and samples were boiled and later sonicated. Approximately 3 × 10^5 cell equivalent per fraction was used for electrophoresis on a 12% SDS-PAGE gel, followed by Western blotting. Densitometry of autoradiogram was done using ImageJ (https://imagej.nih.gov/ij/) to calculate the percentages of FMRP in the nuclear and cytoplasmic fractions. For Western blot whole cell lysates were prepared in lysis buffer [50 mM Tris–HCl pH 7.5/0.5 M NaCl/10 mM $MgCl_2$/1% NP-40/Halt protease

inhibitor cocktail/Halt phosphatase inhibitor cocktail] and at least 20 μg of protein was analyzed by 10% SDS-PAGE before Western blotting. The following antibodies were used: anti-FMRP (Biolegend, 1:1000), anti-Histone H3 (Cell Signaling, 1:500) and anti-GAPDH (Santa Cruz Biotechnology, 1:2000).

In vitro *protein binding assay (for FMRP protein domains and DHX9-His)*

Five micrograms of DHX9-His was incubated with 10 μl Ni-NTA beads in a binding buffer containing 50 mM Tris–HCl, pH 7.5, 150 mM KCl, 10% glycerol, 1 mM EDTA, 1 mM DTT, 0.01% NP-40, 0.1% Tween-20, 10 mM imidazole, and 1 μl benzonase (MilliporeSigma) for 1 h, with mild shaking at 4 °C. The supernatant was removed, and beads were washed three times with 200 μl binding buffer. The binding buffer was completely removed and DHX9-His bound Ni-NTA were further incubated for 15 m with 5 μg FMRP (full length)-WT, N-Fold-WT, N-Fold-I304N, or C-IDR (as indicated in the figures) in 20 μl binding buffer. The protein bound resins were spun down, and the supernatants were taken out carefully. Five microliters of loading buffer was added to supernatants. The resins in each tube were washed three times with 200 μl wash buffer (same buffer with 20 mM imidazole, and 200 mM KCl, without benzonase). The bound proteins were eluted with 25 μl 1X Laemmli buffer. Equal volume of supernatants and the pull-downs were analyzed in 4 to 15% polyacrylamide gradient gel.

R-loop unwinding assay

Two nanometer R-loop with 3′-RNA overhang (5′-γP^{32} labeled) was incubated with 15 nM DHX9 for 30 m at 37 °C in a buffer consisting 10 mM Tris–HCl, pH 7.5, 5 mM $MgCl_2$, 1 mM ATP, 10% glycerol, 0.2 μg/μl BSA, 1 mM DTT, and 1 μl RNasin (Promega), in presence of increasing concentration (25–400 nM) of FMRP-WT, FMRP-I1034N, N-Fold-WT, N-Fold-I304N or C-IDR, as indicated. The reactions were stopped with addition of 1 μl 1% SDS and 1 μl 10 mg/ml Proteinase K (Invitrogen), and incubating at 37 °C for further 5 m. Finally, 2 μl loading buffer composed of 50% glycerol, 20 mM Tris–HCl, pH 7.4, 0.5 mM EDTA, 0.05% Orange G, was added to each tube, and the products were resolved by running in 10% TAE gel, at 100 V for 60 min. The gels were dried, exposed to phosphorimaging screen, and imaged as discussed earlier.

Data availability

All data described herein are contained within the manuscript. This study generated a collection of plasmids, cell lines, and recombinant proteins. All materials will be distributed upon request after publication.

Supporting information—This article contains supporting information.

Acknowledgments—We thank Drs Leszek Kotula, Frank Middleton, Patricia Kane for helpful discussions and Patricia Kane for assistance with microscopic imaging. We thank Dr Helmut Pospiech and Late Dr Frank Große from Leibniz Institute for Age Research - Fritz Lipmann Institute at Jena, Germany for providing P. Sung with the pFastBac-His-DHX9 construct. We also thank Jenny Ha and Charlotte Logan for assisting with cloning of FMRP constructs, Christina Shao for assisting with Western blots, Dattatray Sawant for editing and Nathan McKean for helping with protein purification of FMRP.

Author contributions—A. C. and W. F. conceptualization; A. D., P. S., A. C., R. D., H. H., and W. F. methodology; A. C., A. D., L. G. D., R. D., J. L., L. G., X. X., H. H., P. S., A. B., and W. F. investigation; A. C., A. B., and W. F. writing-original draft; A. C., A. D., L. G. D., R. D., J. L., L. G., X. X., H. H., P. S., A. B., and W. F. writing–review and editing.

Funding and additional information—This work was supported by the National Institute of Health 1R21MH130812 grant and the Department of Defense CDMRP Discovery award W81XWH-15-1-0204 to W. F., the Department of Defense grant PC160083 to H. H., the National Institute of Health grant R35CA241801 to P. S. and the National Institute of Health Award R35GM138097 and The Pew Charitable Trust to A. B. The content is solely the responsibility of the authors and does not necessarily represent the official views of the National Institutes of Health.

Conflict of interest—The authors declare that they have no conflicts of interest with the contents of this article.

Abbreviations—The abbreviations used are: APH, aphidicolin; ATCC, American Type Culture Collection; BSA, bovine serum albumin; ChIP, chromatin immunoprecipitation; co-IP, coimmunoprecipitation; DAPI, 4′,6-diamidino-2-phenylindole; DMSO, dimethyl sulfoxide; eGFP, enhanced green fluorescent protein; FBS, fetal bovine serum; FMRP, fragile X messenger ribonucleoprotein; FXS, fragile X syndrome; IDR, intrinsically disordered region; IgG, immunoglobulin G; KH, K-homology; qPCR, quantitative PCR; PLA, proximity ligation assay; ROI, region of interest.

References

1. Ciaccio, C., Fontana, L., Milani, D., Tabano, S., Miozzo, M., and Esposito, S. (2017) Fragile X syndrome: a review of clinical and molecular diagnoses. *Ital. J. Pediatr.* **43**, 39
2. Sitzmann, A. F., Hagelstrom, R. T., Tassone, F., Hagerman, R. J., and Butler, M. G. (2018) Rare FMR1 gene mutations causing fragile X syndrome: a review. *Am. J. Med. Genet. A* **176**, 11–18
3. Banerjee, A., Ifrim, M. F., Valdez, A. N., Raj, N., and Bassell, G. J. (2018) Aberrant RNA translation in fragile X syndrome: from FMRP mechanisms to emerging therapeutic strategies. *Brain Res.* **1693**, 24–36
4. Sudhakaran, I. P., Hillebrand, J., Dervan, A., Das, S., Holohan, E. E., Hulsmeier, J., *et al.* (2014) FMRP and Ataxin-2 function together in long-term olfactory habituation and neuronal translational control. *Proc. Natl. Acad. Sci. U. S. A.* **111**, E99–E108
5. Zhou, L. T., Ye, S. H., Yang, H. X., Zhou, Y. T., Zhao, Q. H., Sun, W. W., *et al.* (2017) A novel role of fragile X messenger ribonucleoprotein in pre-mRNA alternative splicing through RNA-binding protein 14. *Neuroscience* **349**, 64–75
6. Feng, Y., Gutekunst, C. A., Eberhart, D. E., Yi, H., Warren, S. T., and Hersch, S. M. (1997) Fragile X messenger ribonucleoprotein: nucleocytoplasmic shuttling and association with somatodendritic ribosomes. *J. Neurosci.* **17**, 1539–1547
7. Dockendorff, T. C., and Labrador, M. (2019) The fragile X protein and genome function. *Mol. Neurobiol.* **56**, 711–721
8. Chakraborty, A., Jenjaroenpun, P., Li, J., El Hilali, S., McCulley, A., Haarer, B., *et al.* (2020) Replication stress Induces global chromosome breakage in the fragile X genome. *Cell Rep.* **32**, 108179

9. Thomas, M., White, R. L., and Davis, R. W. (1976) Hybridization of RNA to double-stranded DNA: formation of R-loops. *Proc. Natl. Acad. Sci. U. S. A.* **73**, 2294–2298
10. Crossley, M. P., Bocek, M., and Cimprich, K. A. (2019) R-loops as cellular regulators and genomic threats. *Mol. Cell* **73**, 398–411
11. Garcia-Muse, T., and Aguilera, A. (2019) R loops: from physiological to pathological roles. *Cell* **179**, 604–618
12. Dettori, L. G., Torrejon, D., Chakraborty, A., Dutta, A., Mohamed, M., Papp, C., *et al.* (2021) A Tale of loops and tails: the role of intrinsically disordered protein regions in R-loop Recognition and phase separation. *Front. Mol. Biosci.* **8**, 691694
13. Yang, H., Wang, Y., and Xiang, Y. (2022) FMRP promotes transcription-coupled homologous recombination via facilitating TET1-mediated m5C RNA modification demethylation. *Proc. Natl. Acad. Sci. U. S. A.* **119**, e2116251119
14. Ledoux, N., Gauthier-Naud, W., Lavoie, O., Watters, V., Hussein, S., Adjibade, P., *et al.* (2023) The nuclear isoforms of the Fragile X mental retardation RNA-binding protein associate with genomic DNA bridges. *Mol. Biol. Cell* **34**, ar36
15. Cristini, A., Groh, M., Kristiansen, M. S., and Gromak, N. (2018) RNA/DNA hybrid interactome identifies DXH9 as a molecular player in transcriptional termination and R-loop-associated DNA damage. *Cell Rep.* **23**, 1891–1905
16. Yuan, W., Al-Hadid, Q., Wang, Z., Shen, L., Cho, H., Wu, X., *et al.* (2021) TDRD3 promotes DHX9 chromatin recruitment and R-loop resolution. *Nucleic Acids Res.* **49**, 8573–8591
17. Chakraborty, P., Huang, J. T. J., and Hiom, K. (2018) DHX9 helicase promotes R-loop formation in cells with impaired RNA splicing. *Nat. Commun.* **9**, 4346
18. Smolka, J. A., Sanz, L. A., Hartono, S. R., and Chedin, F. (2021) Recognition of RNA by the S9.6 antibody creates pervasive artifacts when imaging RNA:DNA hybrids. *J. Cell Biol.* **220**, e202004079
19. Hein, M. Y., Hubner, N. C., Poser, I., Cox, J., Nagaraj, N., Toyoda, Y., *et al.* (2015) A human interactome in three quantitative dimensions organized by stoichiometries and abundances. *Cell* **163**, 712–723
20. Dominguez-Sanchez, M. S., Barroso, S., Gomez-Gonzalez, B., Luna, R., and Aguilera, A. (2011) Genome instability and transcription elongation impairment in human cells depleted of THO/TREX. *PLoS Genet.* **7**, e1002386
21. Zang, J. B., Nosyreva, E. D., Spencer, C. M., Volk, L. J., Musunuru, K., Zhong, R., *et al.* (2009) A mouse model of the human fragile X syndrome I304N mutation. *PLoS Genet.* **5**, e1000758
22. Yang, Y., McBride, K. M., Hensley, S., Lu, Y., Chedin, F., and Bedford, M. T. (2014) Arginine methylation facilitates the recruitment of TOP3B to chromatin to prevent R loop accumulation. *Mol. Cell* **53**, 484–497
23. De Boulle, K., Verkerk, A. J., Reyniers, E., Vits, L., Hendrickx, J., Van Roy, B., *et al.* (1993) A point mutation in the FMR-1 gene associated with fragile X mental retardation. *Nat. Genet.* **3**, 31–35
24. Feng, Y., Absher, D., Eberhart, D. E., Brown, V., Malter, H. E., and Warren, S. T. (1997) FMRP associates with polyribosomes as an mRNP, and the I304N mutation of severe fragile X syndrome abolishes this association. *Mol. Cell* **1**, 109–118
25. Jain, A., Bacolla, A., Chakraborty, P., Grosse, F., and Vasquez, K. M. (2010) Human DHX9 helicase unwinds triple-helical DNA structures. *Biochemistry* **49**, 6992–6999
26. Dutta, A., Kwon, Y., and Sung, P. (2022) Biochemical analysis of RNA-DNA hybrid and R-loop unwinding via motor proteins. *Methods Mol. Biol.* **2528**, 305–316
27. Tanner, N. K., and Linder, P. (2001) DExD/H box RNA helicases: from generic motors to specific dissociation functions. *Mol. Cell* **8**, 251–262
28. Chakraborty, P., and Grosse, F. (2011) Human DHX9 helicase preferentially unwinds RNA-containing displacement loops (R-loops) and G-quadruplexes. *DNA Repair (Amst)* **10**, 654–665
29. Zhang, T., Wallis, M., Petrovic, V., Challis, J., Kalitsis, P., and Hudson, D. F. (2019) Loss of TOP3B leads to increased R-loop formation and genome instability. *Open Biol.* **9**, 190222
30. Banani, S. F., Lee, H. O., Hyman, A. A., and Rosen, M. K. (2017) Biomolecular condensates: organizers of cellular biochemistry. *Nat. Rev. Mol. Cell Biol.* **18**, 285–298
31. Forman-Kay, J. D., Kriwacki, R. W., and Seydoux, G. (2018) Phase separation in biology and disease. *J. Mol. Biol.* **430**, 4603–4606
32. Holehouse, A. S., and Pappu, R. V. (2018) Functional implications of intracellular phase transitions. *Biochemistry* **57**, 2415–2423
33. Tsang, B., Arsenault, J., Vernon, R. M., Lin, H., Sonenberg, N., Wang, L. Y., *et al.* (2019) Phosphoregulated FMRP phase separation models activity-dependent translation through bidirectional control of mRNA granule formation. *Proc. Natl. Acad. Sci. U. S. A.* **116**, 4218–4227
34. Sanz, L. A., and Chedin, F. (2019) High-resolution, strand-specific R-loop mapping via S9.6-based DNA-RNA immunoprecipitation and high-throughput sequencing. *Nat. Protoc.* **14**, 1734–1755
35. Ramírez, F., Ryan, D. P., Grüning, B., Bhardwaj, V., Kilpert, F., Richter, A. S., *et al.* (2016) deepTools2: a next generation web server for deep-sequencing data analysis. *Nucleic Acids Res.* **44**, W160–W165